The evolution of quantum confinement in $CsPbBr_3$ perovskite nanocrystals

Justinas Butkus[†], Parth Vashishtha[†], Kai Chen[†], Joseph K. Gallaher[†], Shyamal K. K. Prasad[†], Dani Z. Metin[‡], Geoffry Laufersky[†], Nicola Gaston[‡], Jonathan E. Halpert[*†] and Justin M. Hodgkiss[*†]

† MacDiarmid Institute for Advanced Materials and Nanotechnology, and School of Chemical and Physical Sciences, Victoria University of Wellington, P.O. Box 600, Wellington, New Zealand.

‡ MacDiarmid Institute for Advanced Materials and Nanotechnology, and Department of Physics, University of Auckland, Private Bag 92019, Auckland, New Zealand.

E-mail:
*** Justin.Hodgkiss@vuw.ac.nz**
*** Jonathan.Halpert@vuw.ac.nz**

Contents

1. Synthesis details

Chemicals- Lead(II) bromide (99.999%, Aldrich), cesium carbonate (99%, Aldrich), oleylamine (98%, Aldrich), Oleic Acid (99%, Fluka), 1-Octadecene (90%, Aldrich), cesium bromide (99.999% Aldrich).

Synthesis Method- $CsPbBr_3$ has been synthesized by Colloidal route method adopted from Kovalenko group. Pb(II) bromide, oleylamine and oleic acid were degassed and dissolved in ODE. Cs-oleate was hot injected at particular

temperature, depending on the desired size of nanocrystals. Reaction flask was cooled by iced water after 2 minutes of hot injection.

5 ml ODE and 0.18 mmol $PbBr_2$ (99.999%, Aldrich) were added in a 50 ml 3 neck-flask and degassed for 1 h under vacuum at 120 °C. Simultaneously 0.5 ml oleylamine (98%, Aldrich) and 0.5 ml oleic acid (99%, Fluka) were degassed under same condition separately in a vial and then added in to reaction mixture under N_2. Increase the temperature to 140 °C in order to dissolve OLA and OA with $PbBr_2$ and allow it to dissolve for 30 minutes. Cs-oleate were injected quickly in to the reaction flask at particular temperature (140-175 °C) and reaction flask was cooled down within 10 seconds. The mixing time and hot injection temperature for each sample are provided below.

Sample Name	Mixing time	Temperature
NC-4.1	4 -5 seconds	140 °C
NC-7.3	4 -5 seconds	165 °C
NC-8.6	8 - 10 seconds	175 °C

Table S1. Nanocrystal sample mixing times and hot injection temperatures.

Cs-oleate were synthesize by loading 0.4 gm Cs-carbonate (99%, Aldrich), 15 ml ODE (90%, Aldrich) and 1.2 ml oleic acid (99%, Fluka) in to a 50 ml 3 neck flask. The reaction mixture were degassed for 1h at 120 °C under vacuum and then temperature were raised to 150 °C and heated for 30 minutes in order to react Cs_2CO_3 with oleic acid.

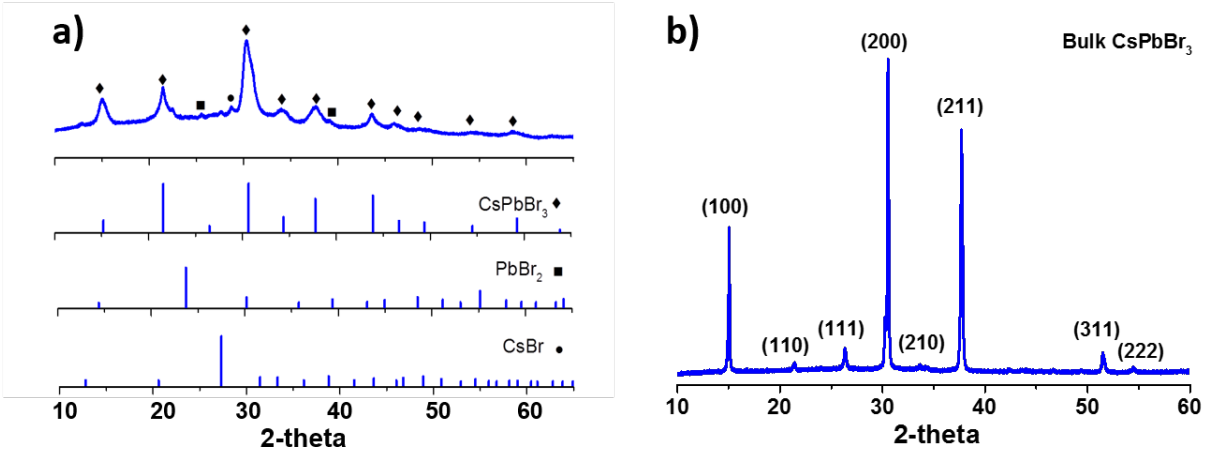

Figure S1. a) XRD Spectra of $CsPbBr_3$ Nanocrystals, b) XRD Spectra of $CsPbBr_3$ Microcrystalline Film. Standard $CsPbBr_3$, $PbBr_2$, and CsBr graphs were taken from Panalytical X'Pert Highscore Plus with the respective reference codes: 04-017-4526, 01-085-1089, and 00-004-0586.

2. Excitation density estimate

Mean excitations per nanocrystal (E_n) were estimated via Eq.1

Equation 1 $$E_n = f\sigma = f\frac{2.303(OD)}{Nl}$$

, where f- pump fluence [photons per cm^2 per pulse], σ- absorption cross section [cm^2], OD- optical density at excitation wavelength measured with Cary 50Bio UV-Vis spectrophotometer, N- nanocrystal concentration [particles/cm^3], l- optical path length [cm].

Nanocrystal concentration was calculated considering $CsPbBr_3$ unit cell volume and molar mass, dry material mass in solution volume and mean cubic particle length obtained via TEM measurements.

Excitation densities obtained matched (~15% uncertainty) the theoretical estimates calculated via complex refractive index as described in the literature.[1-2] Where sample absorption saturation was reached at highest fluence measurements, excitation density was scaled according to the TA signal intensity.

3. Computational Modelling

For density functional theory calculations, Vienna Ab-Initio Simulation Package (VASP) was used. The projector augmented wave (PAW) method was implemented[3], and a cutoff energy of 500 eV was used for the plane wave basis set. The (cubic) lattice parameter was determined to be 5.86 Å. $CsPbBr_3$ in the cubic phase was optimised using the PBEsol functional, allowing the unit cell volume to adjust. The tetrahedron method was used, and an $8 \times 8 \times 8$ Gamma centred k-grid was employed for density of states calculations. The hybrid functional HSEsol[4] was used for density of states and band structure calculations, and spin-orbit coupling was accounted for.

Br-p contributes most heavily to the valence band maximum, with some contribution from Pb-s, while Pb-p contributes heavily to the conduction band minimum (Fig. S2). A larger band gap of 1.43 eV was obtained with the use of PBEsol and no spin-orbit coupling. Inclusion of spin-orbit coupling decreases E_g, to 0.53 eV. This change is due to the lowering of the conduction band, which is caused by spin-orbit splitting of the Pb-p band (Fig. S2). Use of the more accurate screened hybrid density functional, HSEsol, with inclusion of spin-orbit coupling results in a larger band gap of 0.91 eV, as expected due to the inclusion of exact exchange.

Our most accurate value, 0.91 eV, compares only poorly with previous calculations on $CsPbBr_3$ which have found a gap of $E_g = 1.32$ eV. [5] However, we are able to ascribe this difference to the use of a Monkhorst-Pack grid instead of the Gamma centred grid that we have used. The Monkhorst-Pack grid results in a very slow convergence of band gap with the number of k-points, and a difference of 0.79 eV for a $8 \times 8 \times 8$ grid size.

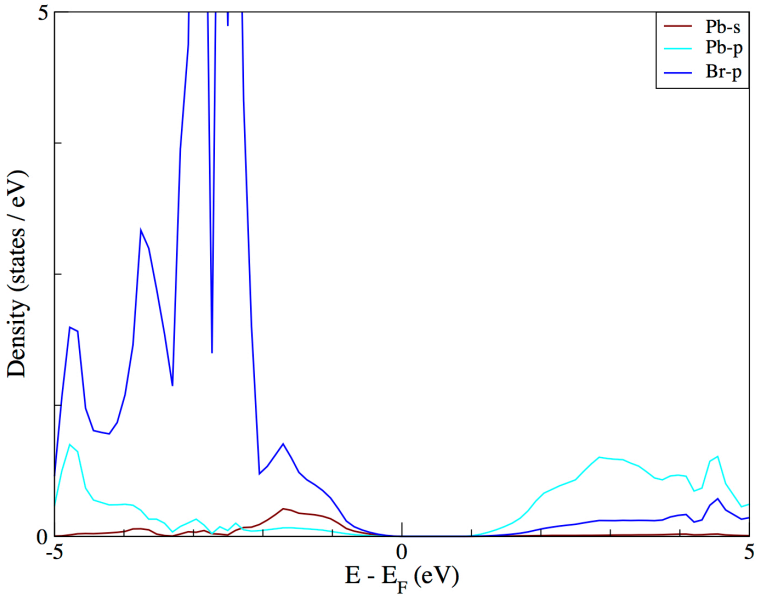

Figure S2. Projected density of states for bulk $CsPbBr_3$, showing the main orbital contributions.

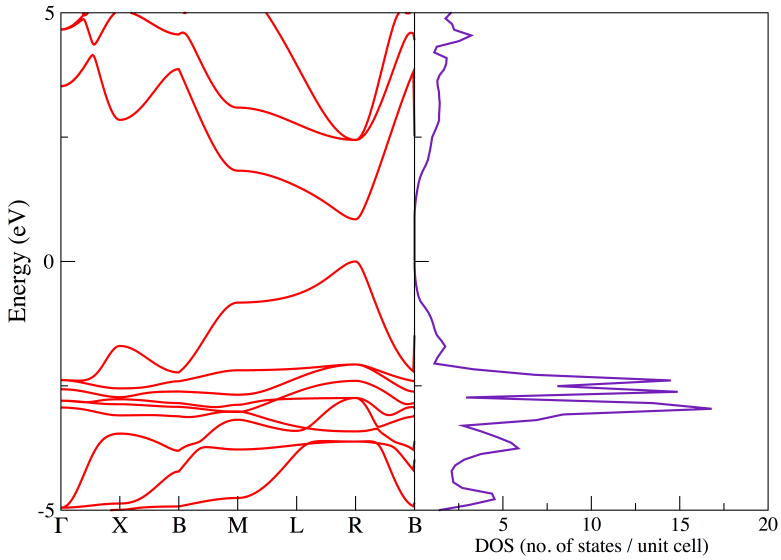

Figure S3. Band structure and density of states for bulk $CsPbBr_3$.

4. Quantum yield measurements

Quantum yield measurements were performed on dilute solutions of NC's (absorbance ~0.05) in anhydrous hexane using a quartz cuvette with path length of 10 mm. An absolute method of determination was employed, using an Edinburgh Photonics FLS980 spectrometer and corresponding integrating sphere.[6] Excitation wavelength was set at 440 nm (10 nm slit width) and the sample and blank hexane spectra were gathered from 420-620 nm (0.54 nm slit width). The excitation intensity was integrated over 425-455 nm of both spectra to determine the portion absorbed photons while integrating over the range of 465-600 nm resulted in the number of emitted photons. The "observed quantum yield" of photons out /

photons in was 31.25%, however it is known that the use of an integrating sphere dramatically increases the sample path length, thus reabsorption events of the high energy edge of the peaks are much more likely.[7] To correct for this, a spectrum was taken from 455-620 nm without the use of an integrating sphere and scaled to tail-match the spectrum from the integrating sphere. The differences in area became a correction factor, yielding the actual quantum yield of 33.85%.

5. Relative cooling dynamics

Carrier cooling dynamics were equated to the spectral evolution of the high energy shoulder of band edge GSB, this perovskite TA feature has been previously show to originate from hot carriers by Price *et al.*[8] The TA spectra at each time point measured was normalized to the band edge bleach and temporal kinetics were extracted as the integral over the high energy spectral evolution region for each of the samples.

6. TA Kinetics

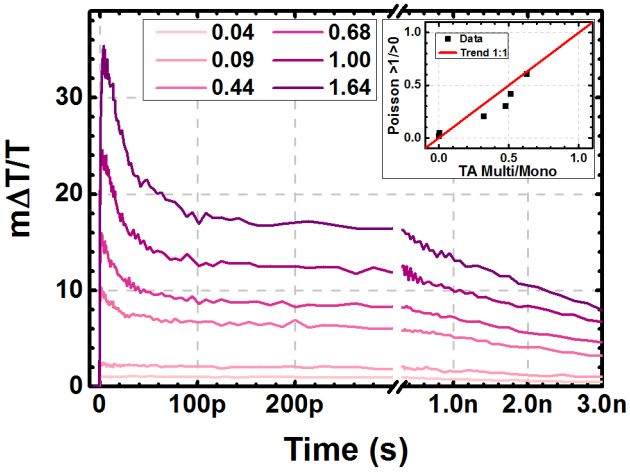

Figure S4. NC-4.1 sample band edge GSB temporal dynamics over varying excitation density. Inset: probability ratio of more than one excitation per NC and probability of 1 or more excitations per nanocrystal vs TA component ratio of multiple excitations and single excitation per NC. The close to 1:1 linear dependence plotted as red line is in agreement with excitation density estimates and their relation to the TA component nature.

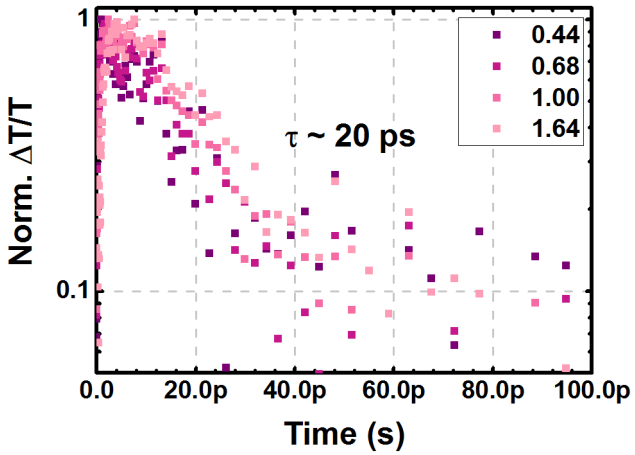

Figure S5. NC-4.1 sample excitation density dependent biexciton dynamics obtained by subtracting the single exciton GSB kinetics contribution, monitored over a wavelength integral over the GSB peak. We note that smaller integrals around the peak region can produce shorter lifetimes.

7. Degeneracy resolution

By considering excitation density proportionality to the TA magnitude we estimate band edge state degeneracy of NC-4.1. Figure S4 shows statistical excitation density contributions of possible degeneracies vs TA signal. The corresponding state degeneracy is expected to have a $\sim x^1$ dependence, where x is TA magnitude. We use Poisson's statistics to obtain an estimate of nanocrystal occupancies at given average excitation densities. We define 'Non-deg' as the case where the band edge state is non-degenerate and depends on probability of >0 excitation/NC; 'Deg = 2', as the case where the band edge state has degeneracy of 2 and depends on nanocrystals with excitations of 1 and (>1*2), where *2 factor corresponds to double contribution to the TA signal; 'Deg = 3', as the case where the band edge state has degeneracy of 3 and depends on nanocrystals with excitations of 1 and (2*2), where *2 factor corresponds to double contribution to the TA and >2*3, where *3 corresponds to triple contribution to TA. The poor linearity of Non-deg case shows that the band edge state is degenerate and the best fitting case with $\sim x^{0.98}$ dependence suggests the degeneracy is 2. However the case where degeneracy is 3 is relatively close to linear dependence with $\sim x^{1.12}$ and Poisson's statistics may be limited at higher excitation densities due to the assumption of independent events, we therefore support this analysis with an additional approach. Figure S5 shows the estimate of band edge TA saturation in relation to the excitation densities. The plotted fit suggests the band edge state of NC-4.1 has a degeneracy of 2.

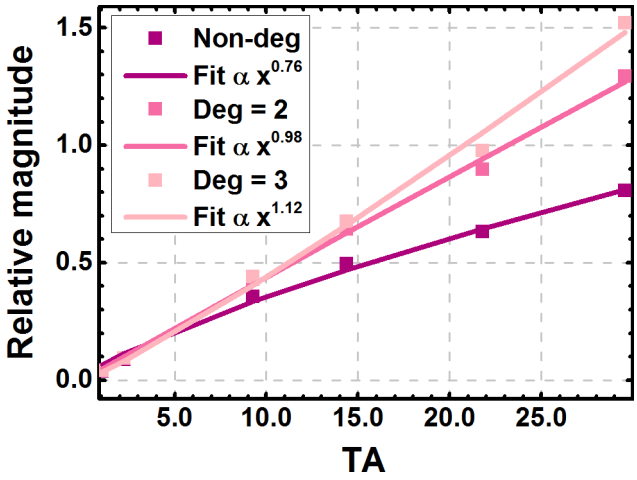

Figure S6. NC-4.1 sample Poisson state contribution estimates vs early time TA estimated over varying excitation fluences. Linearity estimates are plotted as fits with power coefficient given in the legend.

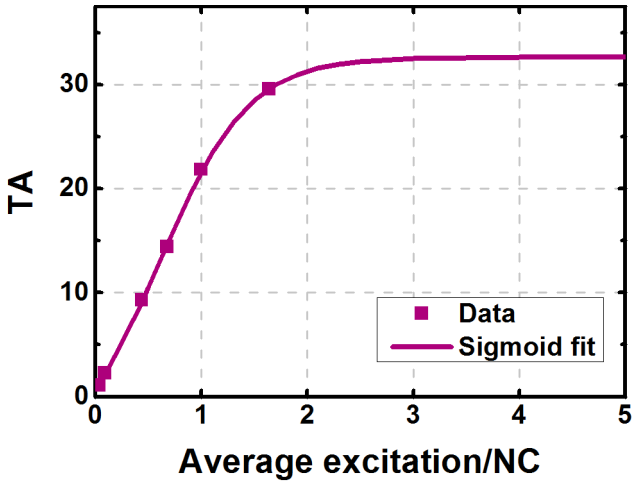

Figure S7. NC-4.1 sample early time TA magnitude vs corresponding average excitation density with free parameter sigmoid fit for saturation estimate.

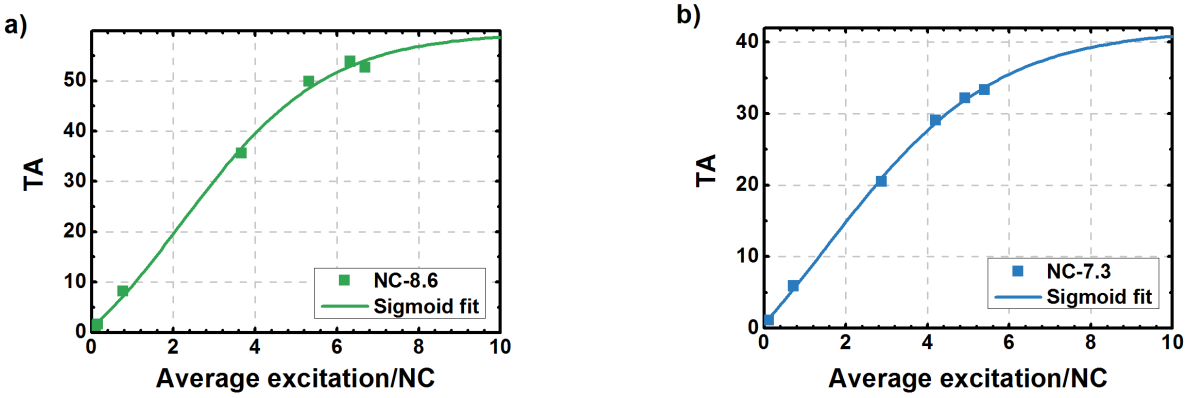

Figure S8. a) NC-8.6 and b) NC-7.3 sample early time TA magnitude vs corresponding average excitation density with free parameter sigmoid fit for saturation estimate.

8. Mott density

Charge carrier screening effect is a mechanism that governs carrier behavior at high excitation densities. It disrupts the excitonic interaction via the presence of Columbic forces from surrounding carriers, impeding electron energy transfer to holes which can reduce available phonon transitions and promote phonon bottleneck effect. When increasing excitation concentration in a material reaches Mott density, exciton interaction disappears due to charge screening and carriers behave like electron-hole plasma. By considering electron-hole system described by classical Boltzmann statistics we calculate the Mott density for bulk $CsPbBr_3$ via Eq. 3.[9]

Equation 2 $$N_M = (1.19)^2 \frac{k_B T}{2a_x^3 E_x}$$

Where ax is the Bohr radius and E_x is the exciton binding energy. At room temperature the $CsPbBr_3$ Mott density is $\sim 1x10^{19}$ excitations/cm^3.

9. TEM micrograph of NC-4.1

Wide angle TEM images confirm the size of the nanocrystals as well as show there is no other population from larger or smaller particles than ~4.1 nm.

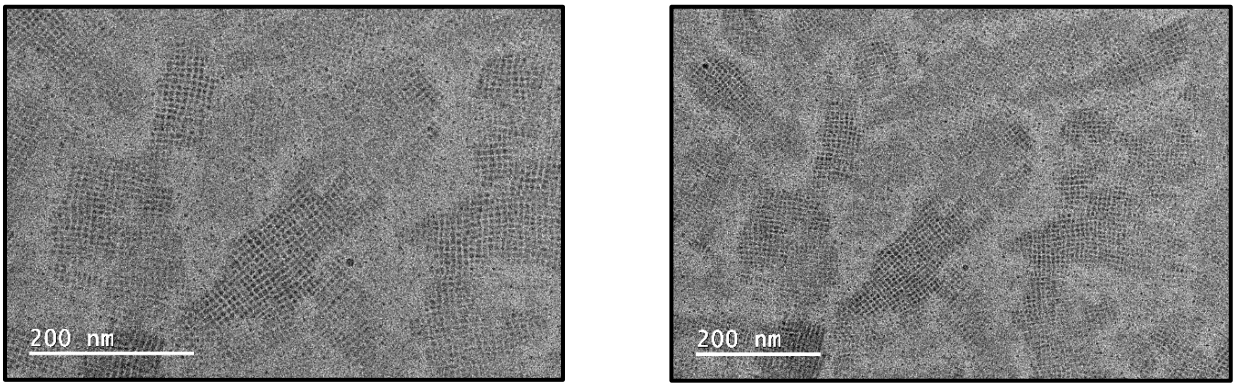

Figure S9. Wide angle TEM images of NC-4.1 sample.

10. UV-Vis absorbance of NC-4.1 before and after washing

Absorption spectra shows that there is no change in the nanocrystals before and after washing by solvent/antisolvent method.

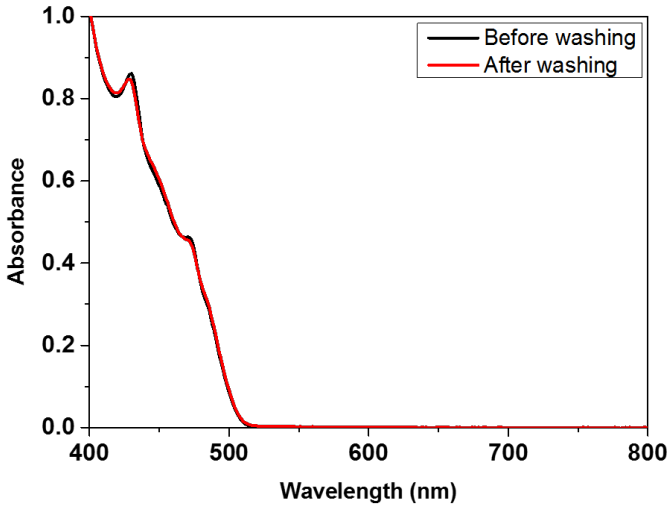

Figure S10. Absorbance spectra of NC-4.1 dispersed in hexane before and after washing.

Acknowledgements

The authors wish to acknowledge the contribution of NeSI high-performance computing facilities to the results of this research. NZ's national facilities are provided by the NZ eScience Infrastructure and funded jointly by NeSI's collaborator institutions and through the Ministry of Business, Innovation & Employment's Research Infrastructure programme. URL https://www.nesi.org.nz. We thank Dr Lukas Hammerschmidt for valuable discussion on theoretical chemistry.

REFERENCES

1. Yu, P.; Beard, M. C.; Ellingson, R. J.; Ferrere, S.; Curtis, C.; Drexler, J.; Luiszer, F.; Nozik, A. J., Absorption Cross-Section and Related Optical Properties of Colloidal InAs Quantum Dots. *J. Phys. Chem. B* **2005,** *109* (15), 7084-7087.

2. Yakunin, S.; Protesescu, L.; Krieg, F.; Bodnarchuk, M. I.; Nedelcu, G.; Humer, M.; De Luca, G.; Fiebig, M.; Heiss, W.; Kovalenko, M. V., Low-threshold amplified spontaneous emission and lasing from colloidal nanocrystals of caesium lead halide perovskites. *Nat. Commun.* **2015,** *6*, 8056.

3. Blöchl, P. E., Projector augmented-wave method. *Phys. Rev. B* **1994,** *50* (24), 17953-17979.

4. Schimka, L.; Harl, J.; Kresse, G., Improved hybrid functional for solids: The HSEsol functional. *J. Chem. Phys.* **2011,** *134* (2), 024116.

5. Lang, L.; Yang, J.-H.; Liu, H.-R.; Xiang, H. J.; Gong, X. G., First-principles study on the electronic and optical properties of cubic ABX3 halide perovskites. *Phys. Lett. A* **2014,** *378* (3), 290-293.

6. Würth, C.; Grabolle, M.; Pauli, J.; Spieles, M.; Resch-Genger, U., Relative and absolute determination of fluorescence quantum yields of transparent samples. *Nat. Protocols* **2013,** *8* (8), 1535-1550.

7. Ahn, T.-S.; Al-Kaysi, R. O.; Müller, A. M.; Wentz, K. M.; Bardeen, C. J., Self-absorption correction for solid-state photoluminescence quantum yields obtained from integrating sphere measurements. *Rev. Sci. Instrum.* **2007,** *78* (8), 086105.

8. Price, M. B.; Butkus, J.; Jellicoe, T. C.; Sadhanala, A.; Briane, A.; Halpert, J. E.; Broch, K.; Hodgkiss, J. M.; Friend, R. H.; Deschler, F., Hot-carrier cooling and photoinduced refractive index changes in organic-inorganic lead halide perovskites. *Nat. Commun.* **2015,** *6*, 8420.

9. Klingshirn, C. F., *Semiconductor Optics*. Springer: 2012.